Analyst

ROYAL SOCIETY OF CHEMISTRY

PAPER

View Article Online
View Journal | View Issue

Cite this: *Analyst*, 2020, **145**, 1337

Ligand structure and charge state-dependent separation of monolayer protected Au_{25} clusters using non-aqueous reversed-phase HPLC†

Korath Shivan Sugi, [a] Shridevi Bhat,[a] Abhijit Nag,[a] Paramasivam Ganesan,[a] Ananthu Mahendranath[a,b] and Thalappil Pradeep *[a]

Received 11th October 2019,
Accepted 3rd January 2020

DOI: 10.1039/c9an02043h

rsc.li/analyst

The synthesis of atomically precise noble metal clusters using various protocols often results in a mixture of clusters with different cores. Hence, it is important to isolate such clusters in their pure form in terms of composition especially for crystallization. High-performance liquid chromatography (HPLC) is a powerful tool to achieve this. The interaction of ligands with column functionalities determine the extent of separation and their stability under conditions used. We demonstrate a systematic flow rate dependent study of three different aliphatic ligand protected Au_{25} clusters, with three commercially available alkyl and aryl functionalized reversed-phase HPLC columns, as they represent the variations encountered commonly. Molecular docking simulations were carried out to understand the interactions between the stationary phase and the cluster surface. These investigations enabled the selection of an appropriate column for better separation of structurally different ligand protected clusters. High-resolution separation of anionic and neutral Au_{25} clusters was acheived with a selectivity (α) of 1.2 by tuning the chromatographic conditions. This study would provide new insights in developing better methods for the efficient separation of monolayer protected clusters.

Introduction

Atomically precise monolayer-protected clusters (MPCs)[1,2] of noble metals are attractive due to their unique size and ligand-dependent properties. Several properties of clusters can be tuned by varying their protecting ligands. Their unique optical absorption,[3] luminescence,[4,5] mechanical,[6] nonlinear,[7,8] and catalytic[9,10] properties can be tailored significantly by using different ligands such as phosphines,[11,12] thiols,[13] alkynyls,[14] and mixed ligands.[15] Among them, the thiolate ligands are widely used, and their structures play a pivotal role in controlling the clusters; in terms of the inner metal core, metal-ligand interfaces having staple motifs. An investigation of three structurally different ligands resulted in clusters having different core and staple motifs with unique optical properties.[16] In this context, knowledge of their total structure is essential to bridge the gap in understanding their properties in detail. The purity of MPCs is a crucial factor affecting the growth of single crystals of clusters and their applications in sensing,[17] imaging,[18] and catalysis.[10,19] There are several methods to purify and isolate MPCs which include fractional precipitation,[20] ultracentrifugation,[21] gel electrophoresis,[22] thin layer chromatography (TLC),[23] size-exclusion chromatography (SEC),[24] and capillary electrophoresis.[25] However, these techniques have certain limitations. In the case of SEC and electrophoresis, selectivity is a major issue.[26]

The reversed-phase high-performance liquid chromatography (RP-HPLC) is an established technique for the high-resolution separation of organic molecules.[27] In 2003, Murray and co-workers separated gold clusters protected with hexane thiol, *N*-acetyl-L-cysteine and tiopronin by RP-HPLC.[28,29] In recent years, Negishi and co-workers have been working extensively on developing new RP-HPLC methodologies for the separation of clusters. They have designed several methods to achieve the separation of clusters according to the number of constituent atoms,[30–32] chemical composition,[33] structural isomers,[19] and coordination isomers.[34] Recently, Knoppe *et al.*, successfully isolated and characterized mass spectrometrically silent $Au_{40}(DDT)_{24}$ clusters[26] using RP-HPLC but, they were not successful in isolating phenylethane thiol protected

[a]*DST Unit of Nanoscience (DST UNS) and Thematic Unit of Excellence (TUE), Department of Chemistry, Indian Institute of Technology Madras, Chennai 600 036, India. E-mail: pradeep@iitm.ac.in*

[b]*Department of Metallurgical and Materials Engineering, Indian Institute of Technology Madras, Chennai 600036, India*

†Electronic supplementary information (ESI) available: Computational details, online UV-vis spectra of clusters in different columns, docked energy minimum conformers of clusters, concentration dependent studies and peak fitting parameters. See DOI: 10.1039/c9an02043h

clusters. Important issues in HPLC based separation of clusters are their solubility and stability, which are predominantly controlled by the protecting ligands. Due to enhanced stability the separation of $Au_{24}Pd$ clusters has been studied extensively.[19,34] Irreversible adsorption of the clusters to column due to the high surface area of the stationary phase can complicate cluster separation.[35] This issue can limit the use of different types of columns for cluster separation. Moreover, the use of buffer solution in the mobile phase can result complications in preparing the mobile phase and shorten the lifetime of the chromatographic columns.[35] However, to achieve higher resolution and better separation, a deeper understanding of the interactions between the stationary phase and the cluster surface is required.

In this work, we have performed a flow rate dependent elution study of three different and commonly used ligand protected Au_{25} clusters, over three standard RP-HPLC columns. We have chosen Au_{25} clusters as model system for our experiments due to their exceptional stability and robustness towards different ligands. The alkyl functionalized C_{18}, C_8, and aryl functionalized phenylhexyl RP-HPLC columns were used. We have also performed molecular docking simulations to understand the noncovalent interactions between the cluster surface and the stationary phase. This study reveals deep insights into the interaction of cluster surfaces having different polarities with alkyl and aryl stationary phases. It also provides helpful information in choosing appropriate columns for the separation of clusters protected with structurally different ligands. We have successfully separated the anionic and neutral Au_{25} clusters from the mixture by optimising the chromatographic parameters.

Experimental

Chemicals

Chloroauric acid trihydrate ($HAuCl_4{\cdot}3H_2O$), dodecanethiol (DDT), octanethiol (OT), phenylethanethiol (PET), tetraoctylammonium bromide (TOAB), and sodium borohydride ($NaBH_4$) were purchased from Sigma Aldrich. The solvents such as tetrahydrofuran (THF), dichloromethane (DCM), and methanol (MeOH) were purchased from Merck and were of HPLC grade. All the chemicals were used as such without any further purification.

Synthesis of $[Au_{25}(SR)_{18}]^-$ clusters

The $Au_{25}(DDT)_{18}$, $Au_{25}(OT)_{18}$, and $Au_{25}(PET)_{18}$ clusters were synthesized according to reported methods.[36] Briefly, 2 mL of 50 mM $HAuCl_4{\cdot}3H_2O$ in THF was diluted to 7.5 mL using THF. To this, about 65 mg of TOAB was added and stirred for 30 min at room temperature. A yellow to deep red color change was observed. About 0.5 mmol of thiol was added to this solution. The deep red color slowly turned to yellow and eventually became colorless after about 45 min. After 2 h, 2.5 mL of ice-cold aqueous $NaBH_4$ (0.2 M) was added. The solution turned black immediately and the reaction was continued for 6 h. The obtained crude cluster solution was evaporated and washed with MeOH repeatedly. After MeOH wash they are extracted in acetone. The acetone fraction was vacuum-dried, and the pure nanocluster was extracted in DCM.

Conversion of $[Au_{25}(SR)_{18}]^-$ clusters to $[Au_{25}(SR)_{18}]^0$

The purified cluster solution in DCM was kept under O_2 environment for 1 h. The oxygen environment was created by an O_2-filled balloon.[37] The oxidation of the clusters was confirmed by monitoring the UV-vis spectrum of the clusters.

Instrumentation

UV-Vis spectroscopy. UV-vis spectra of cluster samples were recorded using a Perkin Elmer Lambda 365 instrument in the range of 200–1100 nm.

MALDI MS measurements. Matrix-assisted laser desorption ionization mass spectrometry (MALDI MS) studies were conducted using an Applied Biosystems Voyager-DE PRO Biospectrometry Workstation. For MALDI MS measurements we have used *trans*-2-[3-(4-tertbutylphenyl)-2-methyl-2-propenylidene] malononitrile (DCTB, >98%) as matrix. Appropriate volumes of the sample and DCTB in DCM were mixed thoroughly, and spotted on the sample plate and allowed to dry at ambient conditions. All the measurements were carried out at the threshold laser fluence in order to minimize fragmentation.

HPLC experiments. HPLC experiments were conducted on a Shimadzu instrument consisting of a CBM-20A controller, DGU-20AR online degasser, LC20AD pump, SIL-20A autosampler, CTO-20A column oven, and SPD-M20A photodiode array (PDA) detector. The stainless-steel columns packed with 5-μm C_{18} bonded silica, (250 × 4.6 mm i.d.) C_8 bonded silica, (250 × 4.6 mm i.d.) and phenylhexyl bonded silica (150 × 4.6 mm i.d.) with a 120 Å pore size (Enable) were used for above experiments. The column temperature was maintained at 28 °C. The absorbance chromatogram was monitored by the photodiode array (PDA) and extracted at 400 nm. The UV-vis spectrum of the eluted peaks was collected over 190–800 nm by the PDA detector. Each sample was dissolved in DCM, *i.e.*, 1.0 mg of the neutral cluster in 1.0 mL of DCM. Then, 30 μL of the sample was injected into the instrument with a mobile phase of 100% MeOH at flow rate varying from 0.5 mL min^{-1} to 2.0 mL min^{-1}. After sample injection, the amount of THF in the mobile phase was continuously increased using a gradient program [10] that increased the [THF]/[MeOH] ratio of the mobile phase from 0% to 100%. The experiments were performed with $Au_{25}(DDT)_{18}$, $Au_{25}(OT)_{18}$ and $Au_{25}(PET)_{18}$ clusters.

Results and discussion

Reversed-phase HPLC is emerging as a widely used technique for the separation of gold clusters. Generally, atomically precise clusters are separated in RP-HPLC by non-aqueous solvents due to their insolubility in aqueous solvents. However, the interaction of the column functionalities with protecting ligands of the clusters, and its effects on their separation and

stability within the column are not adequately known. To understand this aspect, we have investigated the separation of atomically precise gold clusters protected with dodecanethiol, octanethiol, and phenylethanethiol in analytical C_{18}, C_8, and phenylhexyl columns (Fig. S1, ESI†). We will denote them as clusters I, II, and III, respectively in the following discussion. The synthesis of clusters I, II, and III are carried out according to the published procedures[36] and characterized by MALDI mass spectrometry (Fig. S2, ESI†) and UV-vis spectroscopy (Fig. 1a). We have used neutral clusters in our study as anions do not interact actively with the stationary phase.[38] The oxidation of clusters was carried out by keeping them in O_2 environment[37] and the conversion was confirmed from the UV-vis spectrum (Fig. 1a). The neutral cluster solution was injected into the column in DCM and eluted with MeOH–THF as the mobile phase.[19] We have used a linear gradient [10] program as described in Fig. S3† to elute the clusters.[19] In our method, the separation was accomplished in two steps. First, upon injection, the clusters were adsorbed onto the stationary phase (the column) when MeOH was passed, thereby enhancing the interaction of the clusters with the stationary phase. Next, the adsorbed clusters were eluted slowly from the stationary phase depending on their surface polarity. This was accomplished by gradually adjusting the mobile phase from pure MeOH to THF using a linear gradient [10] program. We have used the linear gradient [10] program as increasing the gradient time resulted in peak broadening. In this elution process, the injection solvent was eluted in the initial stage,[19] whose effect was unlikely in the retention process of the clusters. The peaks in the chromatogram were analysed from the online UV-vis spectrum recorded by the PDA detector. The strength of the interaction with the stationary phase is reflected in the retention time (t_R). Scheme 1 shows the schematic representation of the separation process. We have varied the flow rate to understand its dependency on cluster separation. The flow rate was varied from 0.5 mL min^{-1} to 2.0 mL min^{-1}. We haven't used flow rate below 0.5 mL min^{-1} as our interest has been relatively faster isolation. The variation in flow rate can change the eluent volume in a linear gradient [10] program (Fig. S4, ESI†). Fig. 1a shows the UV-visible spectra of anionic and neutral cluster I. The oxidation of cluster I was evident from the increase in the intensity of the 400 nm peak and the dis-

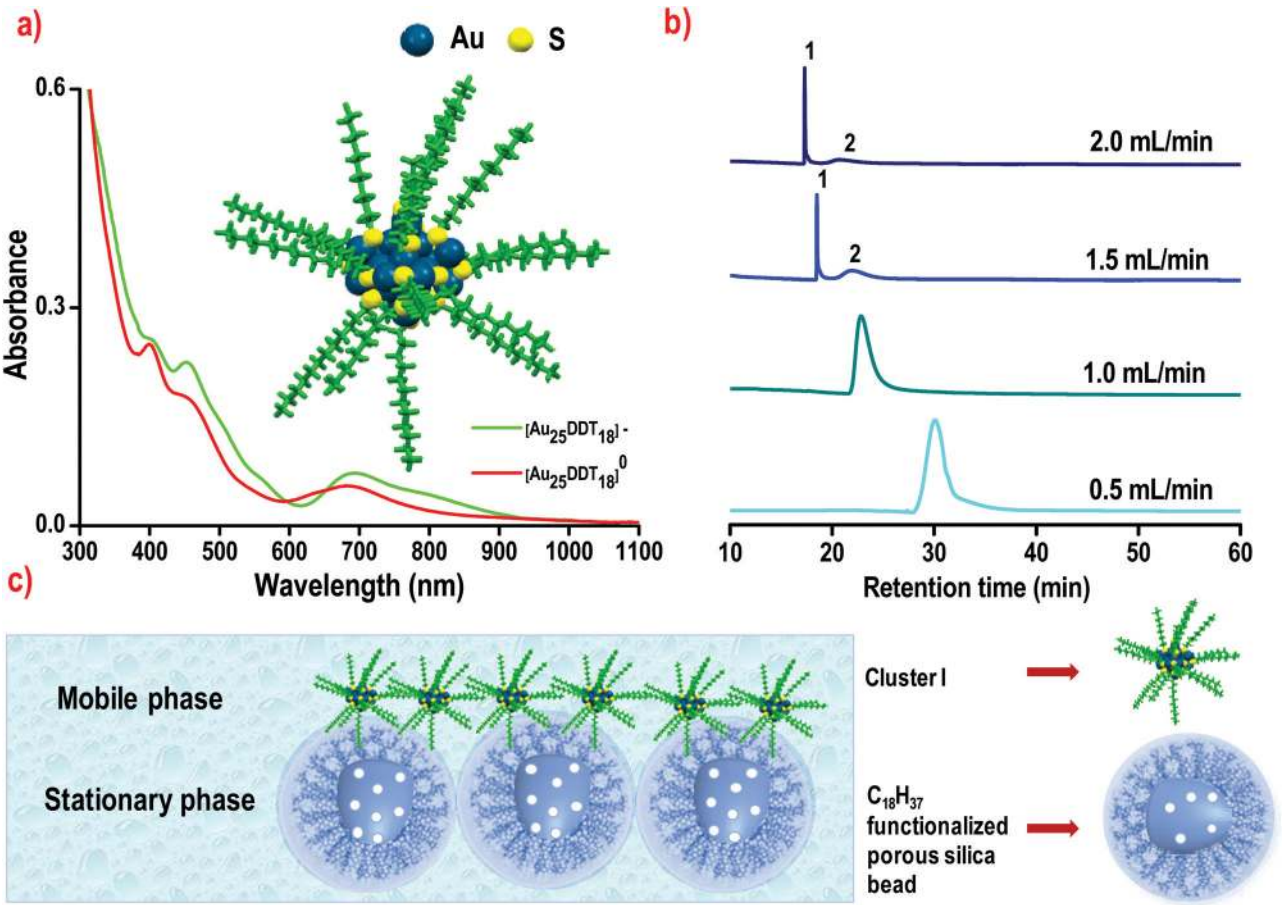

Fig. 1 (a) The UV-vis spectra of anionic (green trace) and neutral (red trace) cluster I. Inset shows the DFT optimized structure of cluster I. (b) Chromatograms of cluster I over C_{18} column, by varying the flow rate. The mobile phase used was MeOH–THF with a linear gradient [10] program. (c) Schematic representation of the strong hydrophobic interaction between the C_{18} functionalized silica beads and the ligands of cluster I. Color labels: teal, Au; yellow, S; green, DDT ligands.

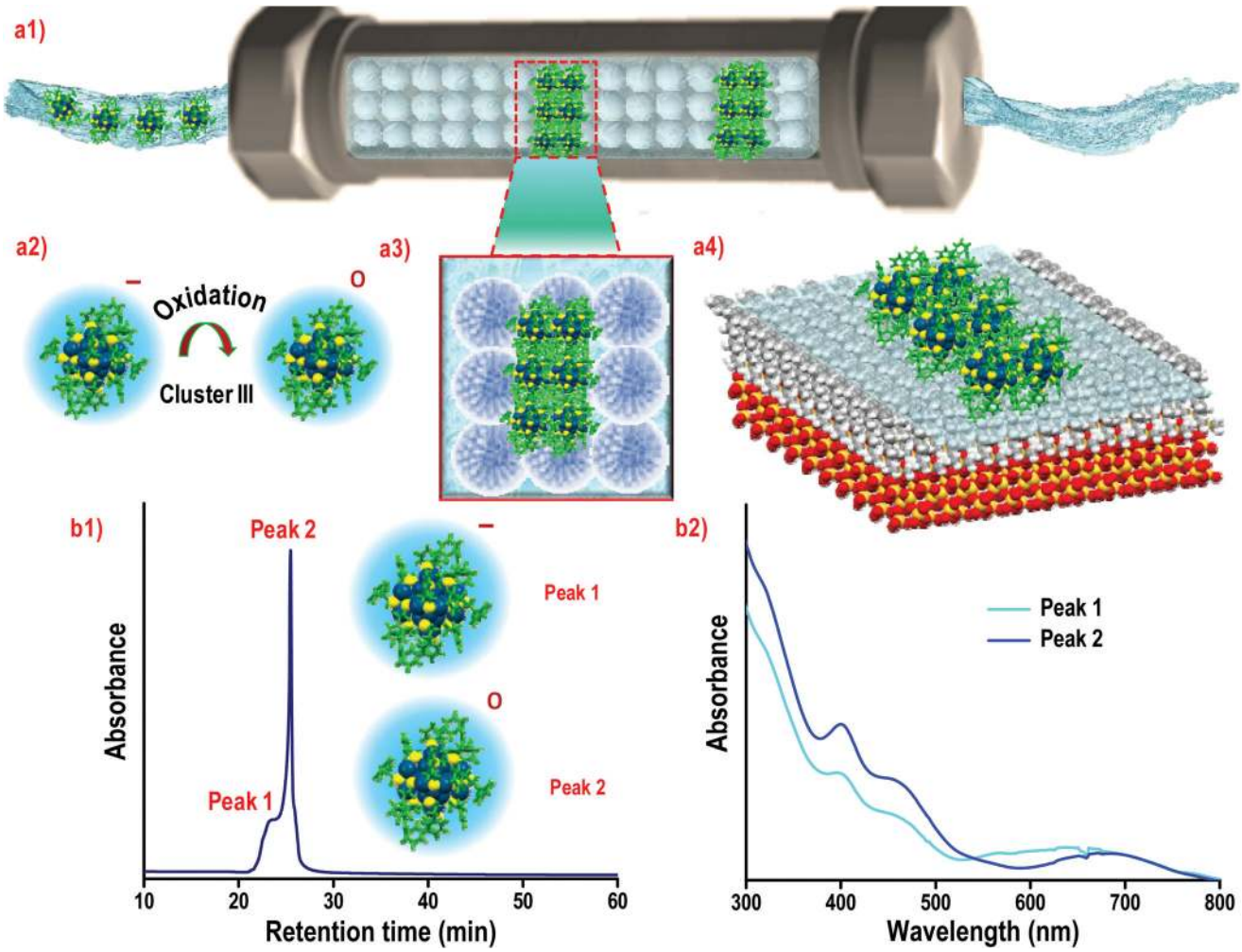

Scheme 1 Separation of Au_{25} clusters in RP-HPLC column. Image a1 is the schematic representation of the separation of Au_{25} clusters over an RP-HPLC column, based on their interaction with the stationary phase. Image a2 represents the oxidation of cluster III. Images a3 and a4 are the enlarged views of silica functionality and clusters. The b1 and b2 are the chromatogram and corresponding UV-vis spectra of the separated bands, respectively.

appearance of the hump at 800 nm. The chromatograms of neutral cluster I eluted at different flow rates are shown in Fig. 1b. The t_R of cluster I at 0.5 mL min^{-1} was 32.28 min. At this flow rate, significant peak broadening and tailing were observed. The characteristic features of Au_{25} clusters was observed in the corresponding online UV-vis spectrum (Fig. S5, ESI†). When flow rate is increased to 1.0 mL min^{-1}, the peak broadening was reduced as compared to the previous case and the clusters were eluted well. At 1.5 mL min^{-1} flow rate, the chromatogram exhibited two peaks which are labelled as peak 1 and 2 (Fig. 1b). The t_R of peak 1 and 2 are at 21.56 and 24.78 min, respectively. The online UV-vis spectrum of peak 2 doesn't show any features of clusters except a broad feature at 680 nm. This could be a decomposed fraction of cluster I which was strongly adsorbed on the column. Similar decomposition was observed in the case of 2.0 mL min^{-1} flow rate. We hypothesize that the strong hydrophobic interaction between long alkyl chain of cluster I and C_{18} functionality of the column (Fig. 1c) might resulted in the decomposition of a small fraction of the cluster. It also indicated that separation was better at an optimum flow rate *i.e.*,1.0 mL min^{-1}. The peak 2 was observed only at higher flow rates which further confirmed that they were decomposed clusters rather than impurities and the peak purity index of peak 1 at 1.5 mL min^{-1} flow rate was 0.96. We have further performed the flow rate dependent elution experiments of other two clusters, *i.e.*, II and III in C_{18} column by keeping all conditions the same. In the case of cluster II, we have observed two peaks up to 1.5 mL min^{-1} flow rate (Fig. 2). The online UV-vis spectra of peak 2 didn't show any characteristic features of the cluster (Fig. S6, ESI†), and this peak was not observed at 2.0 mL min^{-1} flow rate. This indicates that peak 2 may be due to minor impurities[39] present in the cluster as this peak was observed only at lower flow rates. At 2.0 mL min^{-1} flow rate, the elution was very fast and the impurities might be co-eluted along with the clusters which was evident from the reduction in peak purity index to

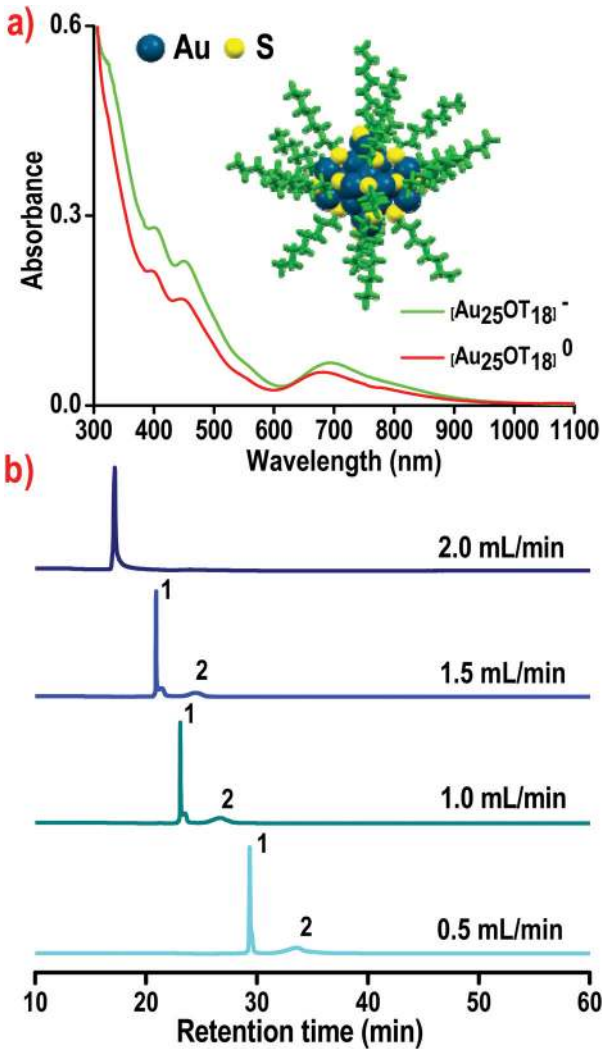

Fig. 2 (a) The UV-vis spectra of anionic (green trace) and neutral (red trace) cluster II. The inset shows the DFT optimized structure of cluster II. (b) Chromatograms of cluster II over C_{18} column by varying the flow rate. Color labels: teal, Au; yellow, S; green, OT ligands.

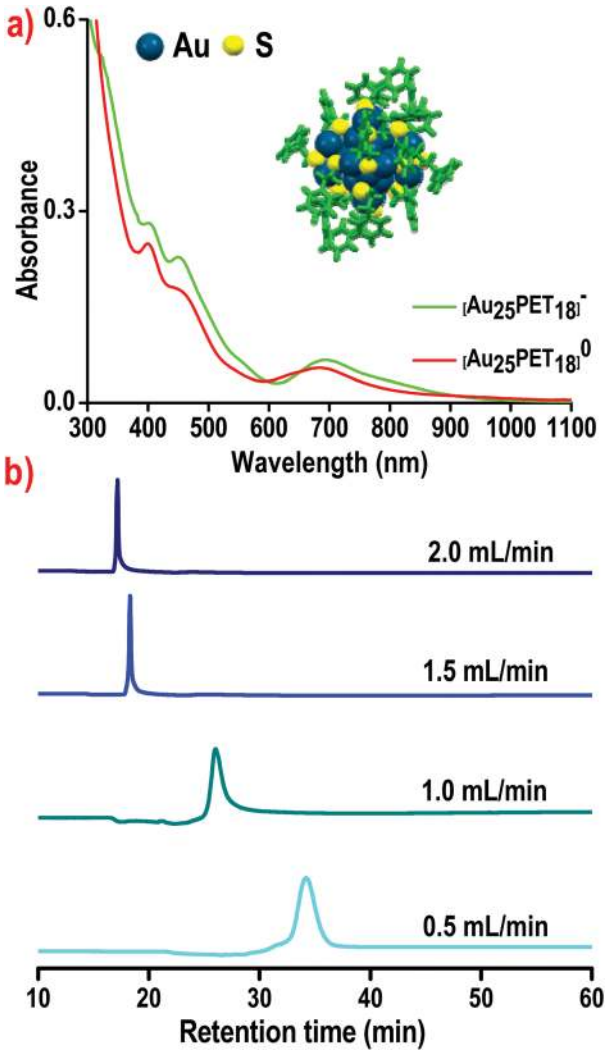

Fig. 3 (a) The UV-vis spectra of anionic (green trace) and neutral (red trace) cluster III. The inset shows the X-ray crystal structure of cluster III. (b) Chromatograms of cluster III over C_{18} column by varying the flow rate. Color labels: teal, Au; yellow, S; green, PET ligands.

0.95. The flow rate dependent study of cluster III in C_{18} column is presented in Fig. 3. We haven't observed any decomposition/impurities of clusters in the chromatograms with increasing flow rate. Also, the peak purity index was 0.98 at 1.5 mL min^{-1}. This observation indicates that the DDT and OT protected clusters bind strongly than that of PET in a C_{18} column (Fig. S7, ESI†). We have carefully analyzed the peak width of each cluster in the C_{18} column. The t_R and peak width (Fig. S8, ESI†) decreases with increase in flow rate. We have conducted similar elution experiments of these clusters with C_8 column under same conditions. All the three clusters were separated well through C_8 column (Fig. S9, ESI†). We didn't observe any flow rate dependent decomposition/impurities, which was further confirmed from the corresponding online UV-vis spectra (Fig. S10, ESI†). But peak broadening was observed in case of cluster III (Fig. S11, ESI†). In our investigation we have explored that the aryl ligand protected clusters are eluting well in all the tested flow rates without decomposition in C_{18} and C_8 columns. So, we extended our flow rate dependent experiments to aryl functionalized phenylhexyl column to understand its effect on cluster separation. We observed that clusters I and II are eluted well (Fig. 4) in all the tested flow rates without any decomposition on this column (Fig. S12, ESI†). In the case of cluster III, the chromatogram of 0.5 mL min^{-1} flow rate shows two peaks, *i.e.*, a small hump at 23.08 min and a peak at 25.47 min which are labelled as peak 1 and 2 in Fig. 5. The online UV-vis spectra of peaks 1 and 2 show features at 400, 450, and 680 nm, but in case of peak 1 the intensity of 400 nm feature was very less compared to that of peak 2. This observation implies that peak 1 and 2 are anionic and neutral cluster III (Fig. 5b). With increasing the flow rate, the small fraction of anionic cluster III present in the solution was transformed entirely into the neutral cluster which was evident from the disappearance of peak 1 in the

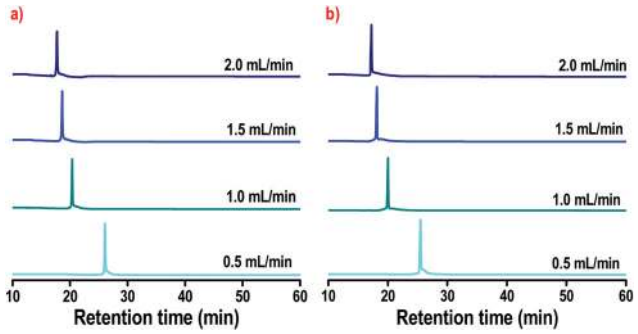

Fig. 4 Chromatograms of cluster (a) I and (b) II at different flow rates over phenylhexyl column.

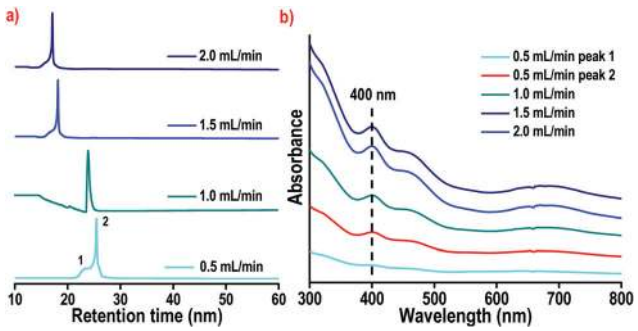

Fig. 5 (a) Flow rate dependent chromatograms of cluster III over phenylhexyl column. (b) The corresponding online UV-vis spectra.

chromatograms at higher flow rates (Fig. 5). Such change in the oxidization state was not observed in the chromatograms of clusters, I and II. This observation implies that the alkyl thiol protected Au_{25} clusters oxidizes fast compared to the PET protected clusters.[40] The peak width analysis of the chromatogram reveals that the peak widths of clusters I and II are lesser than that of cluster III (Fig. S13, ESI†). A plot of the t_R *vs.* flow rate of all the three clusters are shown in Fig. 6. The t_R decreases exponentially with the flow rate, and the data could be fitted with a function of the form $t_R = A^*(\exp(-x/b) + c$ where 'x' is the flow rate in mL min^{-1}. The fitting parameters A, b, and c are listed in Table S1.† This plot provides insights into the interaction of the three structurally different ligand protected clusters with different columns. It is evident from the plot that t_R of clusters I, II, and III in phenylhexyl column are similar, which indicates that the phenylhexyl column separates alkyl and aryl ligand protected clusters with the same efficiency.

We have also tried to separate neutral and anionic Au_{25} clusters from their mixture. For this, a mixture containing 0.5 mg of anionic (labelled as cluster IIIa) and 0.5 mg of neutral cluster (III) in 1 mL DCM was prepared and eluted at 1 mL min^{-1} flow rate. The chromatogram (Fig. 7) shows the high-resolution separation of anionic and neutral cluster which eluted according to their affinity towards the stationary phase (Fig. S14, ESI†). The ratio of retention factor (K) between

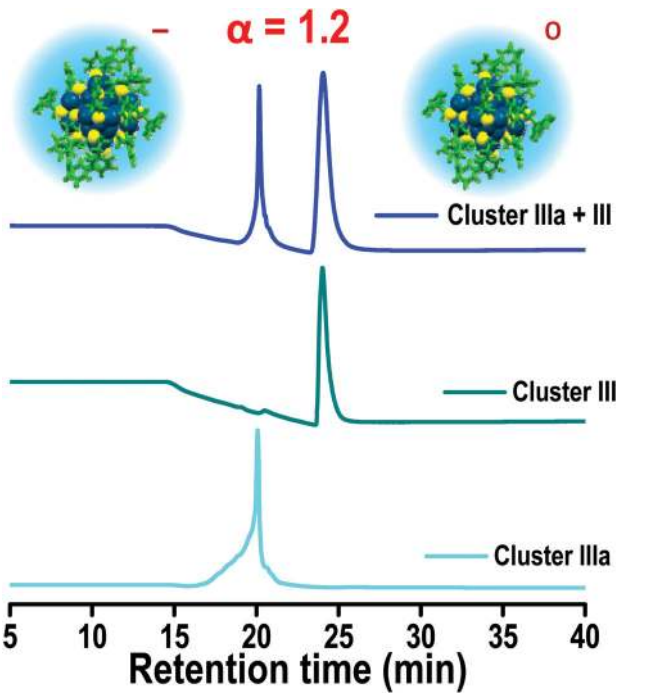

Fig. 7 High-resolution separation of anionic and neutral cluster III over phenylhexyl column at 1 mL min^{-1} flow rate using linear gradient [10] program.

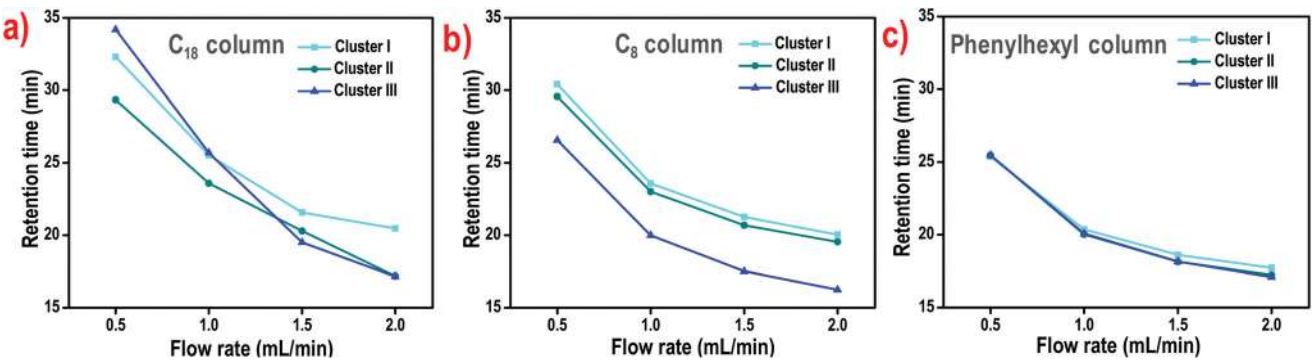

Fig. 6 Variation of the t_R with flow rate of clusters I, II, and III in (a) C_{18}, (b) C_8, and (c) phenylhexyl columns.

Table 1 The binding energies of clusters I, II, and III on C_{18}, C_8, and phenylhexyl columns

Column	Cluster I (kcal mol^{-1})	Cluster II (kcal mol^{-1})	Cluster III (kcal mol^{-1})
C_{18}	−6.09	−2.35	−3.83
C_8	−6.09	−5.99	−10.67
Phenylhexyl	−6.55	−6.02	−8.53

the two peaks is the selectivity 'α' of the HPLC method and it was found to be 1.2.

Molecular docking studies were carried out to understand the interaction of structurally different ligands with the stationary phases used. The docking was performed using the Autodock 4.2 and AutoDock Tools programs.[41] We used the cluster as "ligand", and stationary phase as "receptor" and only the noncovalent interactions were taken into account. The docking study provides information about the binding energies (BE) and the low energy conformations of the stationary phase–analyte complexes. However, the molecular docking study was performed without taking into account the effect of solvent and flow rate used in the real separation. The binding energy values are presented in Table 1. The BE values were negative for all clusters in the RP columns used, revealing that the interaction between stationary phase and cluster are an enthalpy-driven and spontaneous process.[42] The BE of cluster I with C_{18} column was higher compared to that of II and III. The stable low energy confirmations between octadecyl silyl functionality and clusters I, II, and III are shown in Fig. S15.† With C_8 column the BEs of clusters I and II show a similar trend as that of the t_R (Fig. S16, ESI†). In the case of cluster III, the BE is −10.67 kcal mol^{-1} whereas, the t_R is very less for the same. This indicates that the contributions of other factors such as solvent, flow rate, and entropy are inevitable. In phenylhexyl column BEs of clusters I, II, and III are −6.55, −6.02, −8.53 kcal mol^{-1} (Fig. 8). The slightly higher BE value in the case of cluster III could be due to the π–π interactions between the aryl stationary phase and the PET ligand. The BEs (without solvent) obtained by molecular docking were expected to be higher than the experimental results obtained from the HPLC (with solvent) analyse because docking considers enthalpic contribution alone. Nevertheless, a good qualitative agreement was observed, and the docking results may significantly contribute to the understanding of the nature of intermolecular forces responsible for the separation. The factors such as solvent, entropy, and flow rate contributions had to be taken into consideration to obtain the separation quantitatively, which were thought to reduce the differential interaction energy predicted by the simulation study.[43,44] As all the three clusters retain identically in phenylhexyl column, a concentration-dependent elution studies were carried out with cluster III. We have used three different concentrations, *i.e.*, 0.8, 4.0, and 8.0 mg of neutral cluster III, in 1.0 mL DCM by keeping 1.0 mL min^{-1}, as optimum flow rate (Fig. S17, ESI†). The peak area *vs.* concentration shows a linear relationship (Fig. S18, ESI†). With regard to the values of BE and t_R, the aliphatic ligands such DDT and OT protected clusters bind strongly to long chain alkyl functionalised columns which allows the separation of small fractions of decomposed products/impurities whereas, aryl columns are better to separate clusters protected with PET where π–π interactions are involved.

Conclusions

Flow rate dependent elution studies were carried out with three Au_{25} clusters protected with aliphatic ligands using C_{18}, C_8, and phenylhexyl RP-HPLC columns. We observed that the

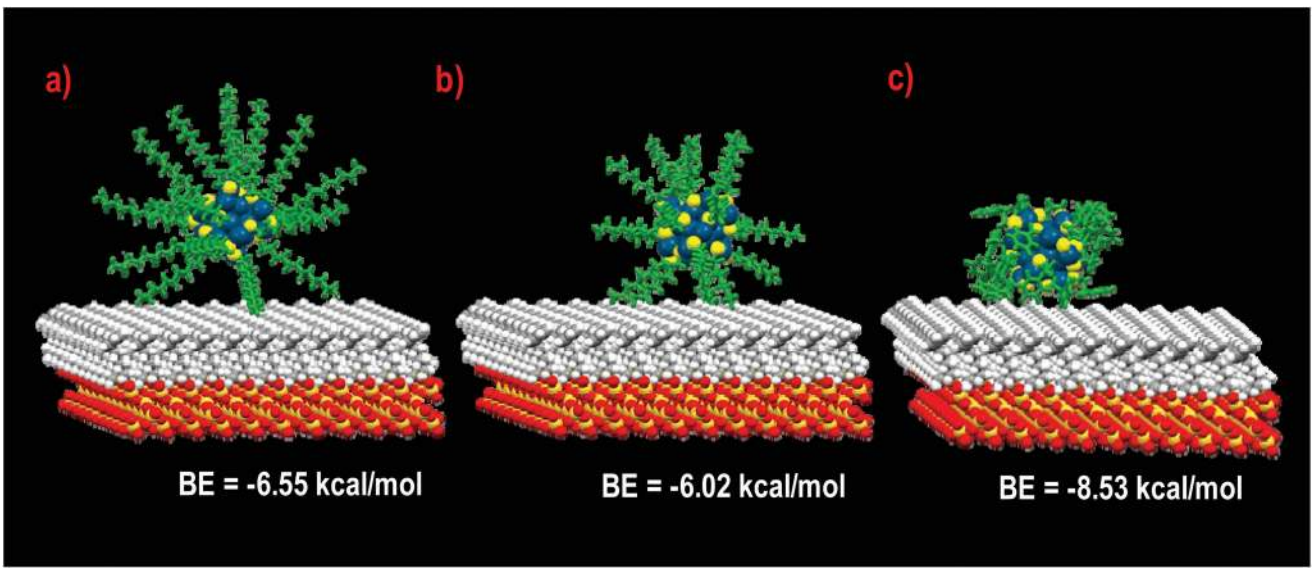

Fig. 8 The energy minimum conformers of phenylhexyl silyl functionality docked with clusters; (a) I, (b) II, and (c) III. Color labels: golden yellow, Si; red, O; grey, C; white, H; teal, Au; yellow, S; green, DDT, OT, and PET ligands.

aliphatic ligands such as DDT and OT protected clusters bind strongly to long chain alkyl functionalised columns which allows the separation of small fractions of decomposed products/impurities whereas, aryl columns are better to separate aryl ligand protected clusters. By tuning the chromatographic conditions, we were able to isolate the neutral and anionic PET protected clusters over the phenylhexyl column with a selectivity of 1.2. The interactions between three clusters and three alkyl and aryl stationary phases were simulated by molecular docking. The experimental findings were corroborated with the binding energy values from the docked structures. We believe that the results of this study provide new insights into the high-resolution separation of structurally different ligand protected metal clusters, and the outcome will help in developing highly efficient cluster separation methods.

Conflicts of interest

There are no conflicts to declare.

Acknowledgements

We thank the Department of Science and Technology, Government of India for constantly supporting our research program on nanomaterials. K. S. S. thanks the University Grants Commission (UGC), Govt. of India for a research fellowship. S. B., A. N. and A. M. thanks IIT Madras for their research fellowships. P.G. thanks IIT Madras for institute postdoctoral fellowship.

References

1 R. Jin, C. Zeng, M. Zhou and Y. Chen, *Chem. Rev.*, 2016, **116**, 10346–10413.
2 I. Chakraborty and T. Pradeep, *Chem. Rev.*, 2017, **117**, 8208–8271.
3 M. Zhu, C. M. Aikens, F. J. Hollander, G. C. Schatz and R. Jin, *J. Am. Chem. Soc.*, 2008, **130**, 5883–5885.
4 A. Mathew, E. Varghese, S. Choudhury, S. K. Pal and T. Pradeep, *Nanoscale*, 2015, **7**, 14305–14315.
5 E. Khatun, A. Ghosh, P. Chakraborty, P. Singh, M. Bodiuzzaman, P. Ganesan, G. Nataranjan, J. Ghosh, S. K. Pal and T. Pradeep, *Nanoscale*, 2018, **10**, 20033–20042.
6 K. S. Sugi, G. Mallikarjunachari, A. Som, P. Ghosh and T. Pradeep, *ChemNanoMat*, 2018, **4**, 401–408.
7 G. Ramakrishna, O. Varnavski, J. Kim, D. Lee and T. Goodson, *J. Am. Chem. Soc.*, 2008, **130**, 5032–5033.
8 S. Knoppe, M. Vanbel, S. van Cleuvenbergen, L. Vanpraet, T. Bürgi and T. Verbiest, *J. Phys. Chem. C*, 2015, **119**, 6221–6226.
9 X.-K. Wan, J.-Q. Wang, Z.-A. Nan and Q.-M. Wang, *Sci. Adv.*, 2017, **3**, e1701823.
10 S. Yamazoe, K. Koyasu and T. Tsukuda, *Acc. Chem. Res.*, 2014, **47**, 816–824.
11 M. S. Bootharaju, R. Dey, L. E. Gevers, M. N. Hedhili, J.-M. Basset and O. M. Bakr, *J. Am. Chem. Soc.*, 2016, **138**, 13770–13773.
12 Y. Shichibu, M. Zhang, Y. Kamei and K. Konishi, *J. Am. Chem. Soc.*, 2014, **136**, 12892–12895.
13 R. Jin, *Nanoscale*, 2015, **7**, 1549–1565.
14 Z. Lei, X.-K. Wan, S.-F. Yuan, Z.-J. Guan and Q.-M. Wang, *Acc. Chem. Res.*, 2018, **51**, 2465–2474.
15 A. Das, T. Li, K. Nobusada, Q. Zeng, N. L. Rosi and R. Jin, *J. Am. Chem. Soc.*, 2012, **134**, 20286–20289.
16 M. Rambukwella, N. A. Sakthivel, J. H. Delcamp, L. Sementa, A. Fortunelli and A. Dass, *Front. Chem.*, 2018, **6**, 330.
17 L.-Y. Chen, C.-W. Wang, Z. Yuan and H.-T. Chang, *Anal. Chem.*, 2015, **87**, 216–229.
18 L. Polavarapu, M. Manna and Q.-H. Xu, *Nanoscale*, 2011, **3**, 429–434.
19 Y. Niihori, M. Matsuzaki, T. Pradeep and Y. Negishi, *J. Am. Chem. Soc.*, 2013, **135**, 4946–4949.
20 P. R. Nimmala, B. Yoon, R. L. Whetten, U. Landman and A. Dass, *J. Phys. Chem. A*, 2013, **117**, 504–517.
21 R. P. Carney, J. Y. Kim, H. Qian, R. Jin, H. Mehenni, F. Stellacci and O. M. Bakr, *Nat. Commun.*, 2011, **2**, 335.
22 T. G. Schaaff and R. L. Whetten, *J. Phys. Chem. B*, 2000, **104**, 2630–2641.
23 A. Ghosh, J. Hassinen, P. Pulkkinen, H. Tenhu, R. H. A. Ras and T. Pradeep, *Anal. Chem.*, 2014, **86**, 12185–12190.
24 S. Knoppe, J. Boudon, I. Dolamic, A. Dass and T. Bürgi, *Anal. Chem.*, 2011, **83**, 5056–5061.
25 C. K. Lo, M. C. Paau, D. Xiao and M. M. F. Choi, *Electrophoresis*, 2008, **29**, 2330–2339.
26 S. Knoppe and P. Vogt, *Anal. Chem.*, 2019, **91**, 1603–1609.
27 I. A. Haidar Ahmad, W. Chen, H. M. Halsey, A. Klapars, J. Limanto, G. F. Pirrone, T. Nowak, R. Bennett, R. Hartman, A. A. Makarov, I. Mangion and E. L. Regalado, *Analyst*, 2019, **144**, 2872–2880.
28 M. M. F. Choi, A. D. Douglas and R. W. Murray, *Anal. Chem.*, 2006, **78**, 2779–2785.
29 V. L. Jimenez, M. C. Leopold, C. Mazzitelli, J. W. Jorgenson and R. W. Murray, *Anal. Chem.*, 2003, **75**, 199–206.
30 Y. Negishi, T. Nakazaki, S. Malola, S. Takano, Y. Niihori, W. Kurashige, S. Yamazoe, T. Tsukuda and H. Häkkinen, *J. Am. Chem. Soc.*, 2015, **137**, 1206–1212.
31 Y. Niihori, D. Shima, K. Yoshida, K. Hamada, L. V. Nair, S. Hossain, W. Kurashige and Y. Negishi, *Nanoscale*, 2018, **10**, 1641–1649.
32 Y. Niihori, C. Uchida, W. Kurashige and Y. Negishi, *Phys. Chem. Chem. Phys.*, 2016, **18**, 4251–4265.
33 Y. Negishi, W. Kurashige, Y. Niihori, T. Iwasa and K. Nobusada, *Phys. Chem. Chem. Phys.*, 2010, **12**, 6219–6225.
34 Y. Niihori, Y. Kikuchi, A. Kato, M. Matsuzaki and Y. Negishi, *ACS Nano*, 2015, **9**, 9347–9356.
35 Y. Zhang, S. Shuang, C. Dong, C. K. Lo, M. C. Paau and M. M. F. Choi, *Anal. Chem.*, 2009, **81**, 1676–1685.

36 Z. Wu, J. Suhan and R. Jin, *J. Mater. Chem.*, 2009, **19**, 622–626.
37 S. Bhat, R. P. Narayanan, A. Baksi, P. Chakraborty, G. Paramasivam, R. R. J. Methikkalam, A. Nag, G. Natarajan and T. Pradeep, *J. Phys. Chem. C*, 2018, **122**, 19455–19462.
38 Y. Niihori, Y. Koyama, S. Watanabe, S. Hashimoto, S. Hossain, L. V. Nair, B. Kumar, W. Kurashige and Y. Negishi, *J. Phys. Chem. Lett.*, 2018, **9**, 4930–4934.
39 M. Galchenko, R. Schuster, A. Black, M. Riedner and C. Klinke, *Nanoscale*, 2019, **11**, 1988–1994.
40 J. Jung, S. Kang and Y.-K. Han, *Nanoscale*, 2012, **4**, 4206–4210.
41 G. M. Morris, R. Huey, W. Lindstrom, M. F. Sanner, R. K. Belew, D. S. Goodsell and A. J. Olson, *J. Comput. Chem.*, 2009, **30**, 2785–2791.
42 Y. Li, D. Liu, P. Wang and Z. Zhou, *J. Sep. Sci.*, 2010, **33**, 3245–3255.
43 H.-W. Tsui, N. H. L. Wang and E. I. Franses, *J. Phys. Chem. B*, 2013, **117**, 9203–9216.
44 B. Zhu, F. Zhao, J. Yu, Z. Wang, Y. Song and Q. Li, *New J. Chem.*, 2018, **42**, 13421–13429.